NATIONAL RADIO ASTRONOMY OBSERVATORY
Green Bank, West Virginia

ELECTRONICS DIVISION INTERNAL REPORT NO. 307

PHASED ARRAY FEEDS FOR LOW NOISE REFLECTOR ANTENNAS

J. Richard Fisher

September 24, 1996

Phased Array Feeds for Low Noise Reflector Antennas

J. Richard Fisher

September 24, 1996

Abstract

Phased array feeds offer the possibility of more efficient use of large radio astronomy reflector antennas by providing more closely spaced beams over a wide field of view and higher aperture efficiency in each beam than have been realized with horn feeds. Phased arrays have been used extensively in rapid scanning radars and shaped-beam satellite systems, but the array design criteria for low-noise radio astronomy antennas are markedly different, particularly as they affect array sampling density. Element spacing in the focal plane must be less than 1λ for large F/D reflectors and less than about 0.7λ for $F/D < 0.5$. This rules out conventional horns as array elements and imposes a limit on the array bandwidth. The receive-only case of radio astronomy permit the use of a number of signal combining techniques that do not degrade system sensitivity. Problems of array weight optimization, mutual coupling, and correction of reflector errors are examined briefly in this paper.

1 Introduction

The straightforward extension of conventional reflector antenna feed techniques to wide fields-of-view is to add more feeds in the reflector focal plane. However, the physical size of even moderately efficient waveguide feeds dictates beam spacings of two or more beamwidths. This leads to an undersampling of the far field power by factor of at least 16 [1], [2]. Also, waveguide feeds are well matched to the focal plane fields only near the optical axis of the telescope. The efficiency loss and beam distortion due to off-axis reflector aberrations can be quite severe.

*J. R. Fisher is with the National Radio Astronomy Observatory, P. O. Box 2, Green Bank, WV 24944, USA. E-mail: rfisher@nrao.edu .

†The National Radio Astronomy Observatory is a facility of the National Science Foundation operated under cooperative agreement by Associated Universities, Inc.

A number of papers have shown that phased array feeds are effective in improving the efficiency of off-axis beams of large-aperture reflectors [3]-[8]. This work is quite relavent to the low-noise reflector feed design problem, but it needs to be extended to optimization on the basis of signal-to-noise ratio with simultaneous closly spaced beams. Very recently, Vilnrotter *et al.* [9] have demonstrated a feed array for optimizing signal-to-noise ratio of a low-noise system in real time. Their work is extended in this paper to include the effects of coherent background noise (spillover) and more complete sampling of the focal plane fields.

Phased array feeds have a long history of development for wide-angle scanning of radar beams [10] and for shaped beams on satellite transmitters [11]-[14], but the design constraints on these systems are considerably different from those on low noise radio astronomy antennas. Transmitting systems are restricted to phase-only beam scanning, and the satellite systems are optimized for transmitted gain over a chosen footprint.

Most array feeds contructed to date have used elements designed to optimally illuminate the reflector as an independent feed. This has resulted in lost power due to array undersampling because of the element spacing restrictions imposed by the element selection. To realize the full potential of a phased array feed, the reflector illumination pattern and secondary beam-forming operation must both be accomplished primarily with optimized complex weights on the element signals and only secondarily with selection of the element radiation pattern. In fact, we will see that the restrictions on element spacing will severely limit the choice of element pattern.

With one exception [9], none of the array feed designs in the literature have taken advantage of the fact that some low noise reflector antenna applications are receive-only, such as distant spacecraft reception or radio astronomy research. This opens up a range of digital signal processing techniques that break some of the constraints previously assumed in array design. The correlation techniques commonly used in aperture synthesis work [15]-[17] may be applied to the array feed problem to reduce data processing speed requirements and to permit data reprocessing to form beams at any spacing and with a variety of sidelobe properties without loss of information. The fundamental limits of beam orthogonality and sampling theory [18]-[20] still apply, but they appear in the guise of correlated signals or noise, instead of power loss.

A number of technical advances such as very low noise, ambient temperature amplifiers, small inexpensive cryogenic refrigerators, and affordable signal processing on a very large scale need to take place before phased array feeds see widespread use in radio astronomy [21], but these will certainly come. At a few frequency ranges the technology already exists to build small arrays that are competitive with low-noise waveguide horn systems.

2 Producing a Far-field Beam from the Measured Coherence Function

From reciprocity, we know that we can transmit a wave with maximum far-field gain by generating an electromagnetic field pattern in the focal plane of a reflector antenna that is everywhere the complex conjugate of the fields produced in the focal plane by a point source in the far-field beam peak. Again, using reciprocity, we can show that the received and transmitted beam shapes are the same, and the field pattern can be conjugately matched in any surface crossed by the ray paths, not just the reflector's focal plane.

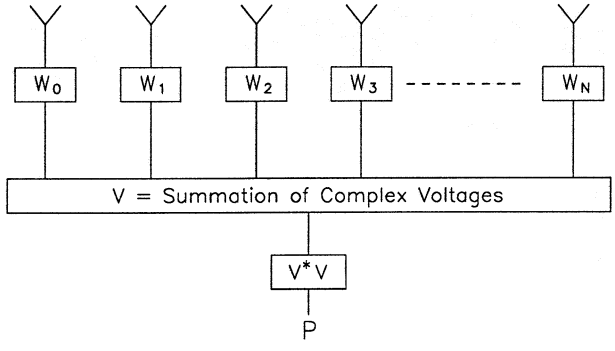

Figure 1: Beam power output by combining signal voltages from a small-element focal plane array.

Let us generate the transmitted field in the focal plane by dividing the power among a large number of electrically small antennas using power dividers and phase shifters to losslessly produce the proper complex weight for each element as shown in Figure 1, ignoring mutual coupling effects for the moment. The same divider network may be used as a combining network in the receiving case to produce a beam output. The mathematical equivalent of the combiner is

$$V = \sum_{i=0}^{N} W_i v_i \tag{1}$$

where W_i is the complex weight applied to the voltage, v_i from element i.

Another method of forming a beam in the receiving case is to measure and combine the vector products of the signals from every element pair in the array as shown in Figure 2. This is the same as measuring the field coherence function

in the surface defined by the array. The relative advantages of these two schemes will be discussed briefly below.

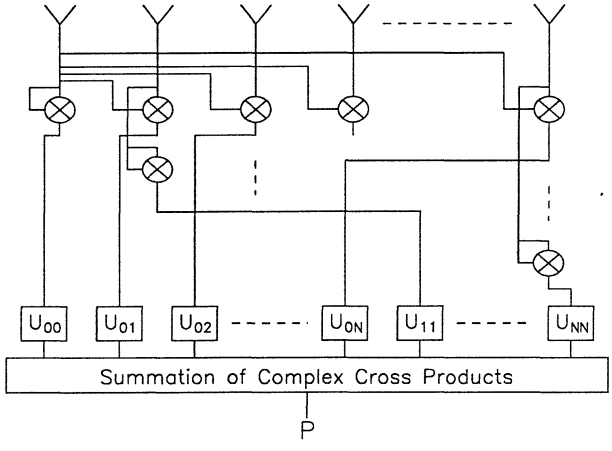

Figure 2: Beam power output from measurements of the focal plane field coherence function.

Comparison of Figures 1 and 2 shows that the element-pair vector products are given by

$$U_{ij}p_{ij} = W_i v_i W_j v_j, \tag{2}$$

where p_{ij} is the measured output of each element pair multiplier, and U_{ij} is now the complex weight to be applied to each multiplier output. With a little algebra

$$\sum_{j=0}^{N} U_{ij}p_{ij} = \sum_{j=0}^{N} W_i v_i W_j v_j = W_i v_i \sum_{j=0}^{N} W_j v_j \tag{3}$$

$$\sum_{i=0}^{N} W_i v_i = \sum_{i=0}^{N} \frac{\sum_{j=0}^{N} U_{ij}p_{ij}}{\sum_{j=0}^{N} W_j v_j} = \frac{1}{\sum_{j=0}^{N} W_j v_j} \sum_{i=0}^{N}\sum_{j=0}^{N} U_{ij}p_{ij}, \tag{4}$$

and the fact that the sum over i is the same as the sum over j, an equation emerges for the conversion of the coherence function measurements to the power output of our array receiver.

$$P = \left[\sum_{i=0}^{N} W_i v_i\right]^2 = \sum_{i=0}^{N}\sum_{j=0}^{N} U_{ij}p_{ij}. \tag{5}$$

For each beam direction of the reflector antenna there will be a different set of coherence weights, U_{ij}. Therefore, the summation in Equation 5 must be done once for each beam direction in the desired field of view.

Equation 5 makes no assumptions about the transfer function from far-field to sample plane, but the problem of determing the U_{ij} matrices remains. If we know enough about the reflector, we can compute its matrices using physical optics. If some of the reflector aberrations are not known *a priori*, the matrices may be solved for with the measured products, p_{ij}, using the "self calibration" technique described by Cornwell and Napier [17].

If we assume that an extensive implementation of either of the beam-forming methods in Figures 1 or 2 in analog hardware is impractical, we are left with a prodigious signal processing task. The main difference between the two methods is the number of hardware components required at each stage in the signal processing path and the data rates at each stage. The two methods require the same number, N, of array elements, amplifiers, anti-aliasing filters, and digital samplers.

The direct voltage combination in Figure 1 requires N_B summing networks and $N_B N_E$ complex multipliers to form the products, $W_i v_i$, where N_B is the number of far-field beams formed, and N_E is the number of elements required to form one beam. Later sections will show that, approximately,

$$19 \leq N_E \leq 100, \tag{6}$$

and

$$(\sqrt{N_B} + \sqrt{N_E})^2 \leq N \leq 1.5(\sqrt{N_B} + \sqrt{N_E})^2. \tag{7}$$

All of these components run at a data rate equal to the RF bandwidth. Since the total number of array elements will always be greater than the number of beams formed, any spectrometer would be attached to the output of the summing network, V, for each beam. Data rate decimation by post detection video filtering must be done *after* the $P = V^*V$ operation.

The field coherence measurement in Figure 2 requires $\sim N_E N/2$ cross-multipliers (correlators), $N_E^2 N_B/2$ complex-weight multipliers ($U_{ij}p_{ij}$) and N_B summation networks. The disadvantage of this configuration compared to the one in Figure 1 is the large number of cross-multipliers and $N_E/2$ times as many weighting multipliers needed. Any generation of spectral information must be done by making each cross-multiplier a multi-delay correlator. Hence, $N_E N/2$, instead of N_B, delay correlators are required for a spectrometer system. The advantage of the correlation method is that, for the cost of an accumulator on the output of each cross-multipler, the data rate in the weighting and summation stages can be greatly reduced. In many cases, the post-correlator part of the beam formation can be done in a general purpose computer.

The data rate reduction in the weighting and complex summation stages of the coherence measurement is $B\tau/N_S$, where B is the RF bandwidth, τ is the accumulation time, and N_S is the number of spectral channels. This can range anywhere from 1 to 10^9, more typically $\sim 10^5$. Another advantage of the slower data rate and an implementation of weights and summation in a general-purpose computer is that the correlation accumulator outputs can be

stored and recombined with a choice of different weights to maximize various far-field beam and system parameters. To do the same reweighting with the direct combining network one would need to save the output from the sampler on each array element. The ratio of storage data rates of the two systems would be $(2N/N_E N_B) \times (B\tau/N_S)$, where $N/N_E N_B \approx 1$. $(B\tau/N_S)$ represents the number of independent samples accumulated per spectral resolution element.

Since the radiation from the sky and the reflector beam pattern orientation usually changes slowly with time, all of the coherence measurements, p_{ij} in Equation 5, do not have to be measured simultaneously. This permits a trade-off between observing speed and the total amount of hardware required to implement the scheme in Figure 2.

Finally, we should note that our assumptions of reciprocity do not preclude the use of amplifiers ahead of the combining network in a receive-only system such as is used in radio astronomy. In fact, losses in combining networks and signal levels needed by practical signal multipliers require considerable gain early in each element's signal path. With sufficient low-noise preamplification there is no signal-to-noise penalty in reusing the signal from each element many times.

3 Array Element Spacing and Size

The field at any point in the focal plane of a parabolic reflector is the vector sum of radiation arriving from all parts of the reflector. Maximum aperture efficiency in this case requires that every element illuminate the entire reflector. For an infinite array, the complex weights in Equation 1 or 5 that produce maximum gain also cancel spillover radiation. In other words, the reflector is uniformly illuminated without spillover if the maximum gain criterion is satisfied. An array of finite size cannot provide maximum gain and minimum spillover simultaneously, so the weights are generally set to maximize the gain to system temperature ratio (G/T) as discussed in Section 5

Neither the maximum gain nor complete spillover cancellation can be achieved if the element spacing is large enough to produce a grating response within the response pattern of a single element. For example, the grating response of an infinite, uniform one-dimensional array will begin to appear at array end-fire when the element spacing is

$$S_0 = \frac{\lambda}{1 + \sin\theta_0}, \tag{8}$$

where θ_0 is the half-angle of the broadside uniform beam pattern produced by something like a $\sin x/x$ voltage distribution to the elements. Equation 8 is simply derived from the property that, in the $x = sin\theta$ dimension, the array beam is $\pm\theta_0$ wide and periodic with a spacing of λ/S. With a finite, one-dimensional array, the spacing given by Equation 8 would put the 6 dB point of the broadside response at θ_0, and the 6 dB point of the grating response off

the end of the array. The same criterion can be applied to a rectangular two-dimensional array. In the examples to follow we shall use $\theta_0 = 48°$, which gives $S_0 = 0.574\lambda$. None of the array properties illustrated depend on this particular value of θ_0, however.

Notice that this grating response criterion is different from two commonly found in the literature, which are that an unwanted grating respose not fall on the reflector or that the grating lobe not appear for any narrow-beam scanning angle. The array feed beam is normally fixed broadside to the array, and it is made very broad ($\pm\theta_0$) by severely tapering the array excitation function.

A better array configuration is one on a hexagonal grid, since this produces the highest two-dimensional density of elements. The first grating response of a hexagonal array appears at an element spacing of

$$S_h = \frac{\lambda}{(1 + \sin\theta_0)\cos 30°}, \tag{9}$$

because the element row spacing is closer by $\cos 30°$ than it is in a rectangular array. Figure 3 shows the two-dimensional radiation pattern of a 4.03λ-radius, 127-element, hexagonal array with an element spacing of 0.67λ and a complex voltage distribution of $W_i = J_1(2\pi r_i)/r_i$, where r_i is the radial distance of the i^{th} element from the center of the array. The array voltage distribution scale length was chosen for this sample pattern calculation so that the spacing is equal to S_h. Hence, the peak level of the six grating responses at the edge of Figure 3 is 6 dB below the central pattern intensity.

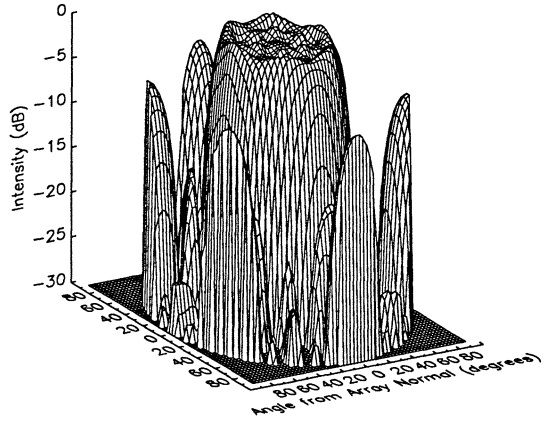

Figure 3: Power pattern of a hexagonal array of semi-isotropically radiating elements spaced 0.67λ. The peak intensity of the six major sidelobes at the outer boundary is -6 dB

When the array is used as a feed for a reflector antenna, the effect of the grating response is to reduce the spillover efficiency of the reflector system and to increase the system temperature from ground radiation pickup. Figure 4 shows the ratio of the power in the main array response to the power in the full hemisphere as a function of element spacing for array patterns like the one shown in Figure 3. The integral ratio is of the form

$$R(s) = \frac{\int_0^{\theta_0} \int_0^{2\pi} E(\theta) A(s,\theta,\phi)\, d\phi\, d\theta}{\int_0^{\pi/2} \int_0^{2\pi} E(\theta) A(s,\theta,\phi)\, d\phi\, d\theta} \tag{10}$$

where s is the element spacing, $E(\theta)$ is the element power pattern, $A(s,\theta,\phi)$ is the array power pattern, and θ_0 has the same definition as above but now appears as the integral limit of the main array response. The limit, $\theta_0 \approx 48°$, was chosen to be at the -9 dB level of the main array response. The solid line in Figure 4 is for semi-isotropically radiating elements ($E(\theta) = 1$). The array size in wavelengths was held constant, and the complex weights of the elements were adjusted to maintain a constant main response width for computing $R(s)$ in Figure 4. The locations of the element spacing limits given by Equations 8 and 9 are marked on this figure.

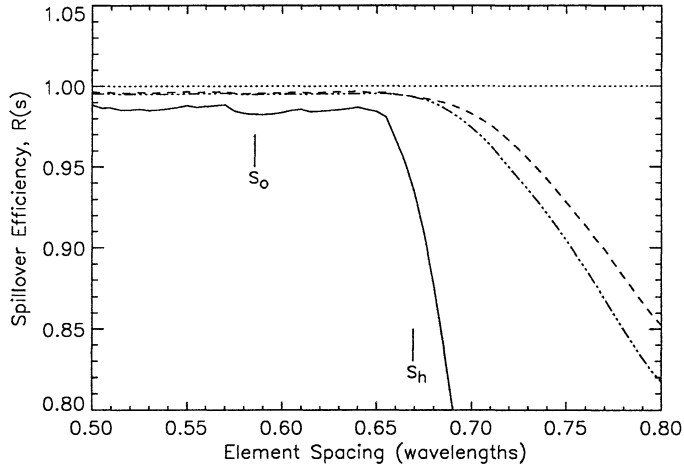

Figure 4: Integral of power pattern in Figure 3 as a function of element spacing assuming a semi-isotropic element radiation pattern (solid line). The dashed line is the same integral using the element power pattern shown in Figure 5. The dash-dotted line is the spillover efficiency with the array weights adjusted to compensate for the element pattern taper (see Section 4). S_0 and S_h are the grating lobe limits given by Equations 8 and 9.

Real antenna array elements do not have isotropic or semi-isotropic radiation

patterns. The restriction of Equation 8 or 9 can be relaxed somewhat because the grating response near the plane of the array will be suppressed by the reduced response of the elements in these directions. The dashed line in Figure 4 shows the spillover efficiency integrals assuming the element radiation pattern shown in Figure 5 and the same θ_0. This particular element pattern is produced by a sinuous planar antenna [22]. The taper introduced to the array pattern by the element pattern is equivalent to the convolution of the array voltage excitation pattern with the field or current distribution of one element.

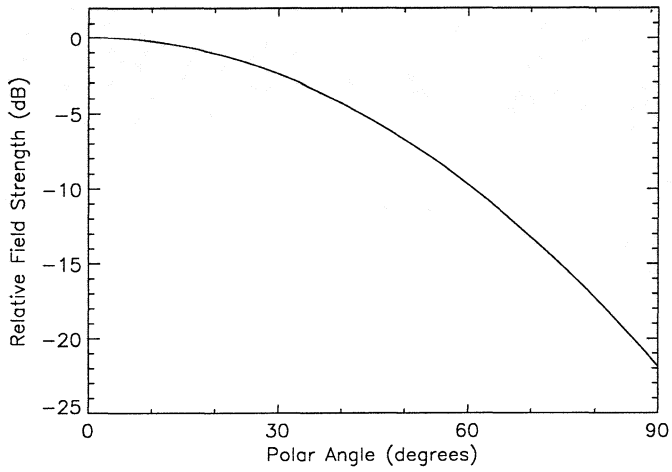

Figure 5: Example element pattern used in computing array spillover efficiency in Figure 4

The physical size of the element assumed in computing the dashed curve in Figure 4 is about $\lambda/2$. This means that the effective bandwidth of such an array is about 0.5:0.7 = 1:1.4. The knee of the dashed curve can be shifted to the right by using elements with a narrower radiation pattern than the one in Figure 5. However, the size of the element must be increased to accomplish this, and this increases the minimum physical spacing of the elements. Hence, the bandwidth remains about the same. Large F/D reflectors with small θ_0 allow larger bandwidths approaching the limit of 1:2.31 as computed by setting $\theta_0 = 0$ in Equation 9.

Can we supress the grating lobe by chosing the proper feed pattern and allow the edge of the grating lobe to just touch the edge of the dish? The answer is yes, only if the physical diameter, d, of the element required is $\leq \lambda/2 \cos 30° \sin \theta_0$. Rahmat-Samii *et al.* [23] present parameterized equations for relating the beam pattern of four likely candidates for array feed elements to their physical size. Of these, the cigar antenna has the smallest size for a given beamwidth. As an example, take a reflector size such that $\theta_0 = 30°$, and require the the edge taper

be -15 dB. From their Figure 1 and Equation 9 we find an element diameter of $\sim 2.1\lambda$, which is nearly twice the allowable diameter of $d = 1.15\lambda$. A similar calculation for $\theta_0 = 45°$, the largest angle given in [23], yields a ratio of physical size to required spacing of ~ 1.7.

This is not to say that waveguide horns cannot be used as phased array elements, as is amply demonstrated by a number of studies and implementations [5],[7],[9],[12]. It just means that these elements cannot simultaneously suppress grating lobes and absorb all of the power crossing the focal plane. Another way of looking at this limitation is that, when the element size (spacing) is large enough to suppress spillover, grating lobes will overlap the main array pattern on the reflector. Then the array excitation function cannot be adjusted to restore uniform illumination of the aperture.

Antenna elements whose size is significantly less than λ break the physical size versus spacing paradox because their pattern approaches $P = \cos\theta$, and they permit spacings such that the grating lobe cannot exist at all. Another way out might be to use end-fire arrays or other super-gain antennas whose transverse size does not change with gain. However, these antennas are rather narrow band and are subject to the fundamental limits of mutual coupling [20] which increases with element gain for a fixed spacing.

4 Field Convolution by Finite Element Sizes

At first thought, array elements of $\lambda/2$ or greater diameter appear to be poor samplers of the focal plane fields because the field reverses phase on the scale of $\lambda F/D$, where F/D is the reflector focal ratio. However, this is not a problem as long as each element has a usable response to the signal from all parts of the reflector. In fact, field convolution due to finite element size can be corrected with appropriate element signal weighting. In other words, the illumination taper due to decreased response of an element to the edge of the reflector can be compensated by the array pattern.

The far field pattern of an array is the product of the point-source array pattern and the pattern of an individual element. Since the electric field in the plane of the array is the Fourier transform of the far field amplitude pattern, the product of the array and element patterns is equivalent to a convolution of the array and element fields in the array plane.

$$E_{elem}(\alpha,\beta)E_{array}(\alpha,\beta) = \int\int (E_{elem}(x,y) * E_{array}(x,y))\, e^{-i\,\delta(x,y)}\, dx\, dy \qquad (11)$$

where $\alpha = \sin(\theta)\cos(\phi)$, and $\beta = \sin(\theta)\sin(\phi)$, and the phase term $\delta(x,y)$ carries the geometric phase delay for each element in the direction (ϕ,θ).

If the array field, $E'_{array}(x,y)$, exists, whose convolution with $E_{elem}(x,y)$ is equal to the ideal array field, then the far field pattern given by Equation 11

will be the same as the array far field without the element taper. This new array field is given by the Fourier transform of the ideal array pattern divided by the element pattern.

$$E'_{array}(x,y) = \int\int \frac{E_{array}(\alpha,\beta)}{E_{elem}(\alpha,\beta)}\, e^{-i\,\delta(\alpha,\beta)}\, d\alpha\, d\beta \tag{12}$$

As long as $E_{elem}(\alpha,\beta)$ has no zeros or very small values where the ideal array pattern is finite, then a usable $E'_{array}(x,y)$ exists. This is illustrated in Figure 6 which shows the far field array pattern with and without element pattern compensation. The dashed curve is computed with $W_i = J_1(2\pi r_i)/r_i$ array weights and an element pattern which is -12 dB at the $\theta = 48°$, a more tapered pattern than shown in Figure 5. The solid curve is computed with the same element pattern but using weights given by Equation 12.

The sharpness of the edge of the array pattern naturally depends on the size of the array in wavelengths. Figure 7 shows array pattern cross sections for three arrays of 4λ, 2λ, and 1.5λ radii. The array sizes chosen for this plot correspond to having 2, 3, and 6 hexagonal rings of elements around the central element. Even one ring (7 elements) can offer significant improvement over the pattern of a single element.

For a given array radius in wavelengths, the detailed shape of the main array response, as shown in Figures 3, 6, and 7, depends weakly (± 1 to ± 2 dB) on the shape of the outer boundary of the array and on element spacing. Since the array voltage distribution is computed from the transform of Equation 12, the far field phase front of the array is, by definition, perfectly spherical. Finite element spacing has no effect on the phase pattern. Any deviation from a spherical wave front in the element pattern, $E_{elem}(\alpha,\beta)$, is corrected through Equation 12.

5 Optimization of Signal-to-Noise Ratio

There are a number of somewhat contradictory criteria that can be used to optimize the element weights of a phased array feed: reflector beam gain, sidelobe level, spillover temperature, reflector beam shape, or signal to noise ratio. The last criterion is the most common one in radio astronomy and is usually stated as maximum G/T, reflector gain divided by system temperature.

Vilnrotter *et al* [9] used a form of the G/T criterion to establish signal weights while allowing for the possibility that each element channel may have a different internal noise temperature. Their signal-to-noise-ratio criterion is identical to the conjugate field match criterion for maximum gain, if one assumes that all channels have the same internal noise. One advantage of their scheme is that they require no *a priori* knowledge of the reflector deformation from a paraboloid. However, their method does not allow for system noise that is coherent from element to element, except to remove it from the calculation of

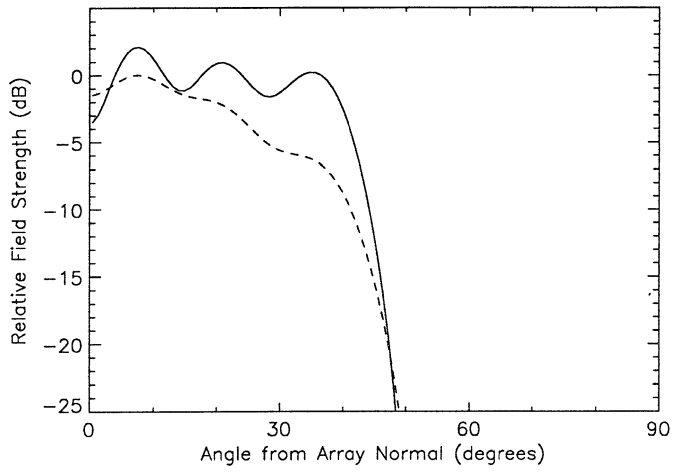

Figure 6: Example of compensation for reflector field taper from the individual element pattern with appropriate array weights. The dashed line is the reflector illumination with an element edge taper of -12 dB. The solid line is the compensated pattern. The reflector half-angle is assumed to be $\theta_0 \approx 48°$. The element spacing is 0.67λ, and the array radius is 4.5λ.

feed weights. They successfully made this simplification because their elements saw very little common spillover noise, but this required that they undersample the focal plane fields as explained in Section 3.

When there is spatially coherent noise in a phased array feed system, the element weights affect the total system temperature much more strongly than they do in the case where all noise, except from the measured radio source, is incoherent. Specifically, we can scale the element excitation pattern to minimize array spillover while maintaining good illumination of the primary reflector as illustrated in Figures 6, 7, and 9.

External noise can be common to two or more array elements and not be spatially coherent. For example, a uniform noise background near the main reflector beam has no spatial coherence to the feed array and, hence, cannot be cancelled with array weights. Spatial coherence can be natural (hemispheric distribution of ground noise) or induced (blocked by the main reflector). Some forms of induced coherence, such as scattering from feed support legs, is of little practical interest because the scale length of the coherence is much greater than size of the feed array. Vilnrotter *et al* reported element-to-element correlation coefficients on blank sky on the order of 0.01, which they tentatively ascribe to atmospheric radiation in the near field of the antenna. There would seem be little spatial coherence from the atmosphere in the main telescope beam, including its near field. More likely sources are primary and secondary reflector

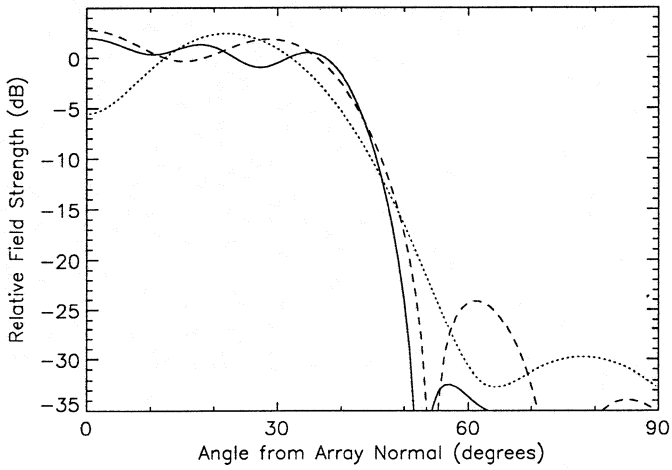

Figure 7: Cross sections of far field patterns of hexagonal arrays of different diameters. The array radii and total numbers of elements are 4λ, 139 elements (solid line); 2λ, 37 elements (dashed line); and 1.5λ, 19 elements (dotted line). In all cases the element spacing is 0.65λ

spillovers which are distributed in sharp rings around the reflectors.

A brute-force search for optimum element weights is impractical, but some powerful simplifying assumptions of axial or planar symmetry can be made for symmetric and offset reflectors, respectively. Then, optimization of G/T is very similar to the same task for a horn feed except that we have much more control over the feed pattern. Start with the most uniform reflector illumination and lowest array sidelobe levels consistent with the array size. Then scale the element excitation pattern in the array linear dimensions for best G/T. Refinement for spillover noise asymmetry can be added without much complication. The spillover efficiency and reflector illumination pattern shown in Figures 4 and 6 indicate that low-noise, high efficiency systems are quite feasible with array feeds. The problems of low amplifier noise and specific optimization of arrays of various sizes are subjects for further work.

It may be worth repeating that optimization can be done after the fact and repeated for different criteria, if the coherece function is recorded as suggested in Section 2.

6 Out-of-Focus Arrays

The feed array is not required to be in the focal plane of the reflector as long as the array intercepts nearly all of the reflected energy, and it adequately samples

the complex field on the surface chosen for the array. In fact, the reflector does not even need to have a focal plane to be a candidate for an array feed. A spherical reflector is a good example [8].

The size of an out-of-focus array will be larger than one of equivalent efficiency near the focus of a paraboloid, but the number of array elements required to properly sample the larger field surface is not necessarily any greater. Figure 8 shows the field phase and amplitude patterns on a surface of rotation whose vertex is 12λ inside the focal point of a 100λ-diameter paraboloid whose focal length is 56λ ($\theta_0 = 48°$). The surface, described by Equation 13, was chosen to be close to a surface of constant phase for a far-field, on-axis source.

$$z = 12.0 - 0.0377r^2 - 1.18 \times 10^{-3} r^3 \tag{13}$$

where z is the distance parallel to the paraboloid axis and r is the distance from the axis, both in wavelengths.

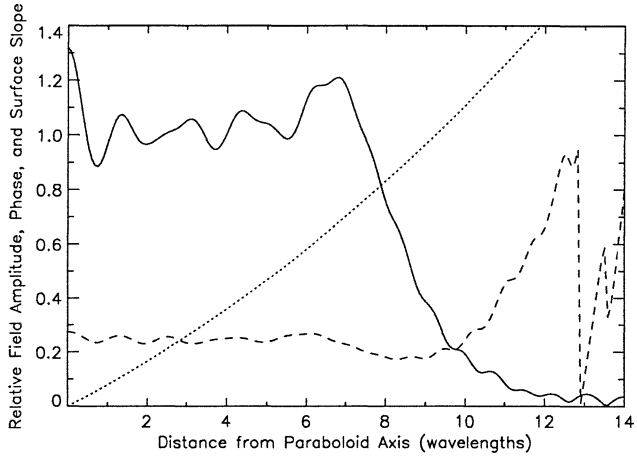

Figure 8: Relative field amplitude (solid line) and phase in wavelengths (dashed line) on the surface described by Equation 13 for a 100λ, $F/D = 0.56$ paraboloidal reflector. The dotted line shows the slope of the array surface to which the element axes are normal.

Since neither the phase nor amplitude changes rapidly across the surface described by Figure 8, the field may be sampled with relatively large elements without undue convolution of the field pattern. Because larger elements have narrower primary beamwidths, this is equivalent to saying that only a limited area of the reflector contributes significantly to the field at any point on the array surface. Hence, each element does not have to see the whole reflector. The narrower element beamwidth is essential to suppressing grating responses that will arise from the larger element spacing.

Figure 9 shows the far-field pattern of an 11λ-radius, 128-element, hexagonal array on the surface described above using an element diameter and spacing of 1.75λ. The element pattern was taken to be the same as in Figure 5 except for scaling in angle by the ratio of 0.5:1.75. Compare this array pattern to the one from the 139-element, 4λ-radius focal plane array shown in Figure 7. We do not have the option of reducing the number of elements further in the out-of-focus array because the element size becomes large compared to the radius of curvature of the array surface.

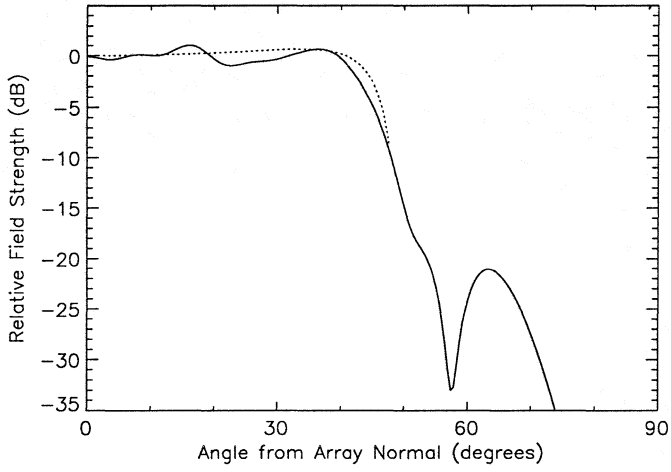

Figure 9: Far-field relative amplitude (solid line) of an 11λ-radius, 128-element, hexagonal array on the surface described by Equation 13 using the phase and amplitudes for each element shown in Figure 8. The dotted line is the reflector aperture taper assumed in computing the fields shown in Figure 8.

One possible advantage of an out-of-focus array such as the one illustrated here is that it has an intrinsically wider bandwidth ratio than the focal-plane array (0.5:1.75 = 1:3.5 instead of 1:1.4). This assumes that a surface of nearly constant phase exists for the reflector and that its radius of curvature is everywhere larger than the element size. It also requires an element whose primary beamwidth scales inversely with frequency. The latter requirement may be impractical for the same reason that the physical size of an element grows faster than its reciprocal beamwidth in the 0.5λ to 2.0λ diameter range as explained in Section 3.

7 Beam Scanning and Surface Error Correction

The reflector fields and array patterns computed in the examples shown so far have assumed perfect paraboloid reflectors and on-axis reflector beams. However, none of the principles that have been used in the calculations depend on these assumptions. Extending the analysis to imperfect reflectors and off-axis beams is a small conceptual step. Changing the complex element weights to match the focal area field from a distorted reflector is straightforward. However, if the fields are substantially redistributed by reflector aberrations the number of array elements required to recombine most of the reflected energy may increase substantially. This, in turn, requires more signal processing power to construct a single beam.

To first order, field patterns near the focal area of a reflector are displaced by $\lambda F/D$ for each half-power beamwidth offset of the reflector beam. In the absence of higher order phase errors, the number of array elements to form one beam remains the same for all beams. The total number of elements required to cover a given image area is the convolution of the single-beam array area with the image area.

However, non-linear aperture phase errors convolve the undistorted focal area field pattern with a function that is the transform of the aperture phase error pattern. The extent to which the focal area fields are spread out depends on the nature of the aperture phase errors [24]. Random surface errors produce a convolving function with an error pedestal whose width is $\sim \lambda F/d$, where d is the characteristic scale length of the surface distortions. If $d \ll D$, the error pedestal is much larger than the undistorted field area, and recovering this power is impractical. The fractional power lost is $1 - \exp(4\pi\epsilon/\lambda)^2$, where ϵ is the illumination-weighted rms reflector surface error [25].

Large scale phase errors, $d \approx D$, produce convolving functions whose width is roughly $\lambda\bar{\delta}F/D$, where $\bar{\delta}$ is the average non-linear phase error in radians. Aberrations well known to optics fall in this category: spherical aberration ($\delta \propto \rho^4$), coma ($\delta \propto \rho^3\cos(\phi)$), and astigmatism ($\delta \propto \rho^2\cos^2(\phi)$), where δ is the aperture phase error, ρ is the aperture radius variable, and ϕ is the aperture azimuthal variable [26]. The focal plane redistribution of intensity due to coma and astigmatism have been computed by Nienhuis and Nijboer [27]-[29] as summarized by Born and Wolf [26] and more recently by Hung and Mittra [30] for coma. Coma is the dominant aberration for off-axis beams of symmetric reflectors [31].

As an example, let us consider the number of 0.5λ-spaced elements in a hexagonal focal plane array required to include 80%, 90%, 95%, and 98% of the reflected power as a function of beam offset. In the results shown in Figure 10 all of the power is assumed to have fallen within a radius of 16λ (5025 array elements) of the offset beam focal spot. Notice that the number of elements required is not quite proportional to the conitguous area necessary to include the stated power fractions, since elements near pattern nulls may be dropped

from the count and outliers near peaks added. Also, optimum reflector sensitivity (maximum G/T) requires somewhat different array configurations from those computed here from purely gain considerations. The computed curves in Figure 10 assume an aperture diameter of 100λ, $F/D = 0.5$, and a mild roll-off of the illumination near the edge of the aperture as given by

$$E_{aperture} = 1.0 - \left[\frac{0.95(2\rho)^2}{D^2}\right]^5 \tag{14}$$

The taper efficiency using Equation 14 is 95%. Both axes in Figure 10 may be roughly scaled to other focal ratios by $(F/D)^2$. With the assumed taper and F/D, the gain loss with a single waveguide feed would be approximately 6 dB at 10 beamwidths offset [32].

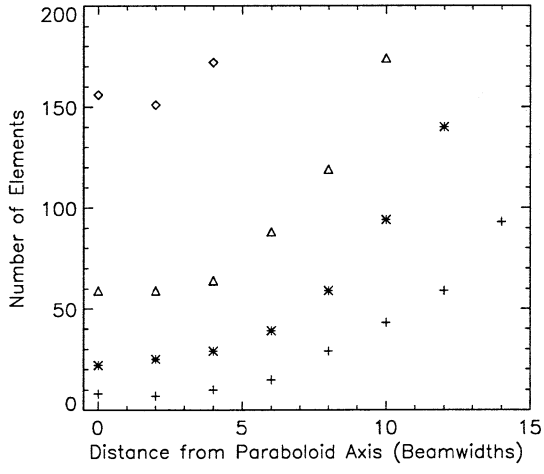

Figure 10: Number of 0.5λ-spaced, hexagonal array elements required to collect 80% (crosses), 90% (stars), 95% (triangles), and 98% (diamonds) of the power passing through the focal plane as a function of beam offset. $F/d = 0.5$, $D = 100\lambda$.

In practice, one might imagine using a signal processor capable of handling a fixed number of elements to form one beam. For example, if that number were 50, Figure 10 shows that the aperture plane efficiency would range from 94% on-axis to about 81% for a 10-beamwidth displacement. This is a considerable improvement on the uncorrected efficiency at this beam displacement.

8 Mutual Coupling

In practice, the elements of a phased array are not completely independent. Any one element will receive power directly from the incoming wave and indirectly

from reflections of this wave from nearby elements. We can express the signal at the terminals of any one element in an array as the sum of direct and indirect signals

$$v_i = \sum_{j=0}^{N} X_{ij} E_j \tag{15}$$

where E_j is the complex field strength at element j, and X_{ij} is the coupling coefficient for a wave scattered from element j to element i. The phase and amplitude of X_{ij} depends on the angle of arrival of the wave, the reflection coefficient of element j, and the coupling coefficient between elements i and j, which may involve secondary scattering from other elements. Because the latter two are very implementation-dependent and not easily computed, only a few solutions of specific cases have appeared in the literature [33], [34]. A few general statements are possible, however.

Pozar [35] showed that, in an infinite array, the far field pattern of an isolated element can be replaced by a pattern that accounts for mutual coupling for the purpose of computing the far field array pattern as given by the left hand side of Equation 11. If the equivalent pattern is not near zero anywhere in the directions of interest, an array excitation function can be computed through Equation 12 to compensate for mutual coupling. The infinite array assumption is invalid for a real array, but one is led to conjecture that an array excitation function exists, equivalent to the one in Equation 12, which takes array boundary effects into account as long as none of the embedded elements in the array has a null in a direction of interest. The study by Steyskal and Herd [36] lends support to this conjecture.

Some types of arrays, such as waveguide apertures in an conducting plane [34], are unsuitable for use as array feeds because they have inherent nulls in their far field patterns due to mutual coupling. Other types of arrays, such as isolated dipoles [37], are inherently null-free, but the introduction of supports can create null-producing mutual coupling.

In the absence of an analytical or numerical solution of the mutual coupling properties of promising array elements, an empirical approach seems feasible. This assertion is bolstered by examples of successful wide-scanning, dense, radar and radio astronomy arrays. A small array, possibly one-dimensional, can be built using the exact element geometry intended for the final array to check for unacceptable mutual coupling effects. The far field pattern of individual embedded elements may then be measured in the final array. These patterns can then be used in a finite-array equivalent of Equation 12 to determine the optimum array excitation function for each beam of the reflector system.

9 Summary

Low noise, receive-only reflector antennas impose significantly different design criteria and present more signal processing possibilities compared to those normally accepted in the design of wide-scanning-angle transmitting antennas. In particular, low spillover is of great importance to low noise antennas, losses in weighted-signal combining networks may be overcome with preamplification, and cross-correlation techniques may be used in the beam forming process. Phased array feeds offer the possibility of more efficient use of large radio astronomy reflector antennas by providing more closely spaced beams over a wide field of view and higher aperture efficiency in each beam than have been realized with conventional feeds.

The main conclusions of this paper are:

- Array element cross-correlation signal processing is equivalent to RF signal combining for beam forming and offers processing speed and flexibility advantages. Beam forming may be done in digital hardware and repeated with different signal weights, if the correlation function is integrated and stored. The signal processing power required for high efficiency, large field of view arrays is very high.

- The bandwidth of a phased array feed in the reflector focal plane is limited to the range 1:1.3 to 1:2 for small and large F/D reflectors, respectively, due to grating lobes. Corresponding element spacings at the high frequency limit of the band are 0.65λ and 1λ. The minimum spacing is about 0.5λ due to mutual coupling.

- Conventional feed horns as array elements cannot realize the full potential of phased array feeds because their physical diameters are at least a factor of two greater than the element spacing required.

- The taper efficiency of an array feed may be greater than the taper efficiency of a single element with appropriate element signal weights.

- A good approximation to optimization of G/T may be done by simply searching the linear array weighting scale length with only one or two free parameters after an initial weighting function is computed from the reflector angle and element pattern.

- Out-of-focus arrays are feasible, and reflector aberrations may be fully corrected as long as the array is large enough to intercept an acceptable fraction of the reflected power.

- Mutual coupling between the elements will affect the array pattern, but this should be correctable by changing array signal weights, as long as the coupling is not so severe that it introduces pattern nulls on the reflector. Practical arrays without nulls have been demonstrated in the literature.

10 Acknowledgements

My thanks to Tim Cornwell and Peter Napier for a number of very helpful discussions. Thanks, too, to Mike Davis, Paul Goldsmith, Mark McKinnon, and Bruce Thomas for comments on various drafts.

References

[1] Johansson, J. F., "A comparison of some feed types," pp. 82-89 in *Multi-feed Systems for Radio Telescopes*, Eds. Emerson, D. T., Payne, J. M., Astronomical Society of the Pacific Conference Series, Vol. 75, 1995

[2] Padman, R., "Optical fundamentals of array feeds," pp. 3-26 in *Multi-feed Systems for Radio Telescopes*, Eds. Emerson, D. T., Payne, J. M., Astronomical Society of the Pacific Conference Series, Vol. 75, 1995

[3] Rudge, A. W. and Davis, D. E. N., "Electronically controllable primary feed for profile-error compensation of large parabolic reflectors," *Proc. IEE*, vol. 117, pp. 352-358, Feb. 1970.

[4] Rudge, A. W. and Withers, M. J., "New technique for beam steering with fixed parabolic reflectors," *Proc. IEE*, vol. 118, pp. 857-863, July 1971.

[5] Galindo-Israel, V., Lee, S-W., and Mittra, R., "Synthesis of a laterally displaced cluster feed for a reflector antenna with application to multiple beams and contoured patterns," *IEEE Trans. Antennas Propagat.*, vol. AP-26, pp. 220-228, Mar. 1978.

[6] Mrstik, A. V. and Smith, P. G., "Scanning capabilities of large parabolic cylinder reflector antennas with phased-array feeds," *IEEE Trans. Antennas Propagat.*, vol. AP-29, pp. 455-462, May 1981.

[7] Blank, S. J. and Imbriale, W. A., "Array feed synthesis for correction of reflector distortion and vernier beamsteering," *IEEE Trans. Antennas Propagat.*, vol. AP-36, pp. 1351-1358, Oct. 1988.

[8] Amitay, N. and Zucker, H., "Compensation of spherical reflector aberrations by planar array feeds," *IEEE Trans. Antennas Propagat.*, vol. AP-20, pp. 49-56, Jan. 1972.

[9] Vilnrotter, V., Fort, D., and Iijima, B., "Real-time array feed compensation system demonstration at JPL," pp. 61-73 in *Multi-feed Systems for Radio Telescopes*, Eds. Emerson, D. T., Payne, J. M., Astronomical Society of the Pacific Conference Series, vol. 75, 1995

[10] Mailloux, R. J., "Hybrid antennas," Chapter 5, Vol. 1, *The Handbook of Antenna Design*, Eds. Rudge, A. W., Milne, K., Olver, A. D., Knight, P., Peter Peregrinus, Ltd., 1982

[11] Rahmat-Samii, Y. and Lee, S-W., "Directivity of planar array feeds for satellite reflector applications," *IEEE Trans. Antennas Propagat.*, vol. AP-31, pp. 463-470, May 1983; correction in *IEEE Trans. Antennas Propagat.*, vol. AP-32, p. 762, July 1984.

[12] Haro, L. de, Besada, J. L., and Galocha, B., "On the radiation of horn clusters including mutual coupling and the effects of finite metal plates: Applications to the synthesis of contoured beam antennas," *IEEE Trans. Antennas Propagat.*, vol. AP-41, pp 713-722, June 1993.

[13] Newell, P. and Bird, T. S., "Effects of mutual coupling in the design of high-performance multifeed satellite antennas," *Radio Science*, vol. 29, pp 145-152, Jan.-Feb. 1994.

[14] Chang, D-C., Hu, C-N. Hung, C-I, Ho, K-T., "Pattern synthesis of the offset reflector antenna system with less complicated phased array feed," *IEEE Trans. Antennas Propagat.*, vol. AP-42, pp. 240-245, Feb. 1994.

[15] Davies, D. E. N., Corless, K. G., Hicks, D.S., and Milne, K., "Array signal processing," Chapter 13, Vol. 2, pp. 359-371, *The Handbook of Antenna Design*, Eds. Rudge, A. W., Milne, K., Olver, A. D., Knight, P., Peter Peregrinus, Ltd., 1982

[16] Thompson, A. R., Moran, J. M., and Swenson, G. W., Jr., *Interferometry and Synthesis in Radio Astronomy*, Krieger Publishing Co., Malabar, FL, 1991

[17] Cornwell, T. J. and Napier, P. J., "The focal plane coherence function of an imaging antenna and its use in measuring and correcting aberrations," *Radio Science*, Vol. 23, pp. 739-748, Sep.-Oct. 1988.

[18] Allen, J. L., "A theoretical limitation on the formation of lossless miltiple beams in linear arrays," *IEEE Trans. Antennas Propagat.*, vol. AP-9, pp. 350-352, July 1961.

[19] Stein, S., "On cross coupling in multiple-beam antennas," *IEEE Trans. Antennas Propagat.*, vol. AP-10, pp. 548-557, Sep. 1962.

[20] Hannan, P. W., "The element-gain paradox for a phased array antenna," *IEEE Trans. Antennas Propagat.*, vol. AP-12, pp. 423-433, July 1964.

[21] Fisher, J. R., "Feed arrays as they affect the design of very large collecting area radio telescopes," pp. 27-33, in *Multi-feed Systems for Radio Telescopes*, Eds. Emerson, D. T., Payne, J. M., Astronomical Society of the Pacific Conference Series, Vol. 75, 1995

[22] DuHamel, R. H. and Scherer, J. P., "Frequency-independent antennas," Ch. 14, pp. 53-82, *Antenna Engineering Handbook*, Third Ed., Johnson R. C. Ed., McGraw Hill, New York, 1993.

[23] Rahmat-Samii, Y., Cramer, P. Jr., Woo, K., Lee, S-W., "Realizable feed-element patterns for multibeam reflector antenna analysis," *IEEE Trans. Antennas Propagat.*, vol. AP-29, pp. 961-963, Nov. 1981.

[24] Napier, P. J. and Cornwell, T. J., "Self-calibration of antenna errors using focal plane arrays," pp. 48-57, in *Multi-feed Systems for Radio Telescopes*, Eds. Emerson, D. T., Payne, J. M., Astronomical Society of the Pacific Conference Series, Vol. 75, 1995

[25] Ruze, J., "Antenna tolerance theory – A review," *Proc. IEEE*, vol. 54, 633-640, 1966.

[26] Born, M., and Wolf, E., Ch. 9, *Princ. of Optics*, Third Ed., Pergamon Press, New York, 1965.

[27] Nijboer, B. R. A., Thesis, Univ. of Groningen, 1942.

[28] Nienhuis, K., Thesis, Univ. of Groningen, 1948.

[29] Nienhuis, K., and Nijboer, B. R. A., *Physica*, vol. 14, 599, 1949.

[30] Hung, C. C. and Mittra, R., "Secondary pattern and focal region distribution of reflector antennas under wide-angle scanning," *IEEE Trans. Antennas Propagat.*, vol. AP-31, p756-763, Sep. 1983.

[31] Ruze, J., "Lateral-feed displacement in a paraboloid," *IEEE Trans. Antennas Propagat.*, vol. AP-13, 660-665, Sep. 1965.

[32] Imbriale, W. A., Ingerson, P. G., and Wong, W. C., "Large lateral feed displacements in a parabolic reflector," *IEEE Trans. Antennas Propagat.*, vol. 22, pp. 742-745, Nov. 1974.

[33] Mailloux, R. J., "Periodic arrays," Chapter 13, pp. 45-49, *Antenna Handbook*, Lo, Y. T. and Lee, S. W., Eds, Van Nostrand Reinhold Co., New York 1988.

[34] Knittel, G. H., Hessel, A., and Oliner, A. A., "Element pattern nulls in phased arrays and their relation to guided waves," *Proc. IEEE*, vol. 56, 1822-1836, Nov. 1968.

[35] Pozar, D. M., "The active element pattern," *IEEE Trans. Antennas Propagat.*, vol. AP-42, pp. 1176-1178, Aug. 1994.

[36] Steyskal, H. and Herd, J. S., "Mutual coupling compensation in small array antennas," *IEEE Trans. Antennas Propagat.*, vol. AP-38, pp. 1971-1975, Dec. 1990.

[37] Chang, V. W. H., "Infinite phased dipole array," *Proc. IEEE*, vol. 56, pp. 1892-1900, Nov. 1968.